

Charged particle emission from ^{194}Hg compound nuclei: Energy and spin dependence of fission-evaporation competition

M. Rajagopalan

*Department of Chemistry, State University of New York at Stony Brook,
Stony Brook, New York 11794*

D. Logan, Jane W. Ball, and Morton Kaplan

Department of Chemistry, Carnegie-Mellon University, Pittsburgh, Pennsylvania 15213

Hugues Delagrange,* M. F. Rivet,[†] John M. Alexander, and Louis C. Vaz

*Department of Chemistry, State University of New York at Stony Brook,
Stony Brook, New York 11794*

M. S. Zisman

Lawrence Berkeley Laboratory, Berkeley, California 94720

(Received 18 August 1981)

Twelve reactions have been studied that produce the compound system $^{194}\text{Hg}^*$ at excitation energies of 57–195 MeV and with l_{crit} values of 25–142 \hbar . Beams of ^{12}C , ^{19}F , ^{20}Ne , and ^{40}Ar ions in conjunction with appropriate targets have been used to measure cross sections for evaporative H/He, fission, and evaporation residues. These results confirm that most ^1H and ^4He is evaporated prior to fission or instead of fission and very little if any from the fission fragments. The probability of H/He evaporation increases dramatically with excitation energy. The evaporation residue cross sections ($\sigma_{\text{ER}}/\pi\lambda^2$) indicate fission survival for entrance channel l up to 27–39 \hbar . Fission survival becomes stronger and corresponding fission competition becomes weaker for excitation ≥ 100 MeV; a connection with charged particle emission is suggested. The dimensionless cross section for evaporation residue ($\sigma_{\text{ER}}/\pi\lambda^2$) depends on both the entrance channel and on energy, indicating that nonequilibrium mechanisms must play an important role, even for $l \lesssim 40$. Heretofore evaporation residue production has been usually thought to arise from lower partial waves while direct reactions have been thought to dominate only for the higher partial waves.

NUCLEAR REACTIONS $^{12}\text{C} + ^{182}\text{W}$; $^{20}\text{Ne} + ^{174}\text{Yb}$; $^{40}\text{Ar} + ^{154}\text{Sm}$;
 $^{19}\text{F} + ^{175}\text{Lu}$; reactions forming $^{194}\text{Hg}^*$ at excitation energies 57, 80, 100,
142, 195 MeV. Measured cross sections for fission and evaporation resi-
dues, evaporative H and He including some energy spectra. Discuss re-
lationship to statistical evaporation model.

I. INTRODUCTION

Reactions between complex nuclei often give rise to intermediate transient systems with very high spins and excitation energies. Their subsequent deexcitation involves competition between fission and evaporation of neutrons, protons, alpha particles, etc., and finally γ -ray emission.^{1–3} In order to probe the mechanisms of mass, energy, and angular momentum transfer in deeply inelastic reactions, measurements have been and are being made of the energy and angular distributions of these emitted nucleons, particles, and γ rays.⁴ The interpretation

of such measurements requires a great deal of information about the statistical properties of excited nuclei.⁵ Systematic studies of reactions that proceed via the complete-fusion mechanism are the primary sources of this information. Projectiles of intermediate mass (e.g., ^{12}C , ^{40}Ar , etc.) have been shown to be most effective for forming the equilibrated compound systems that are needed.

Our group has made a series of studies^{6–9} of the reactions of Au with ^{40}Ar , ^{86}Kr , and ^{136}Xe . Often highly excited targetlike fragments Au^* have been formed and their decay observed via H/He emission or sequential fission. In order to better understand

these observations we have embarked on a parallel series of studies of fission-evaporation competition in compound-nucleus reactions by measuring cross sections for fission, H/He emission, and evaporation residues.^{10,11} We have selected the compound system $^{194}\text{Hg}^*$ as typical of Au^* and easily produced by many target-projectile combinations. In this paper we follow up an earlier Letter¹⁰ with a phenomenological analysis of the cross-section data. In a separate communication¹¹ we discussed, for the ^{40}Ar reactions, the more extensive pattern of the fusion cross sections and the direct emission of H/He. Also separately we will present additional information on the energy spectra observed in the various reactions and make comparisons to statistical-model calculations.

We have followed the established strategy of forming the same compound nucleus through several entrance channels.¹² As we determine the cross sections for fusion (evaporation residues plus fission) along with those for evaporative H/He emission, we obtain a pattern of the cumulative decay fractions (CDF) for $^{194}\text{Hg}^*$ versus the initial excitation energy and average spin. This pattern has intrinsic value for improving our understanding of nuclear deexcitation, testing the applicability of equilibrium theory at high energies, and a particular supplementary value for assisting in the interpretation of studies of deeply inelastic reactions.

II. EXPERIMENTAL ARRANGEMENTS

Beams of ^{12}C , ^{19}F , and ^{20}Ne have been provided by the 88-inch cyclotron and ^{20}Ne and ^{40}Ar by the SuperHILAC at the Lawrence Berkeley Laboratory. Self-supporting targets of ^{182}W , ^{175}Lu , ^{174}Yb , and ^{154}Sm were used and their thicknesses measured by comparison of the elastic scattering with that from an Au target of known thickness (determined by weight and alpha-particle energy-loss measurements). Fission and evaporation residue (ER) products were measured by a gas-ionization telescope¹³ (GT) (≈ 20 Torr of methane and 300 μm Si stopping detector) and H/He by a solid state telescope (SST) (45 μm , 500 μm , 5 mm Si detectors). The GT (solid angle 0.1 to 0.2 msr) could be used at angles as small as 3° to the beam for ER measurements. Often a second GT (1–2 msr) was used for fission product measurements. For measurements of H/He in the SST (3–10 msr) the back angles were emphasized to test for evaporative decay. For angles larger than the grazing angle only thin cover foils (0.2–10 mg/cm² Au or Pb) were used for the

SST, and the laboratory energy thresholds were ≈ 2 and ≈ 8 MeV for ^1H and ^4He , respectively. In Refs. 10 and 11 we showed a number of the angular distributions.

In the more recent experiments (^{40}Ar and ^{20}Ne beams) we mounted two GT's and two to four SST's in the reaction chamber together and recorded data from four or five of these simultaneously. Irradiation times and intensities were planned primarily for measurements in the singles mode (several hundred ER events per run, hundreds to thousands of fission events per run, three to twenty thousand H and He per run). Often coincidences between fission and H/He were also recorded and they provide some additional information on the nature of the evaporationlike emissions. Some results from these coincidence studies are reported in Refs. 10 and 11; others will soon be published.

III. EXPERIMENTAL RESULTS

The general features of the observed energy and angular distributions for H/He have been given elsewhere.^{8–12,14,15} Very similar behavior has been observed for all the reactions studied; namely, there is strong forward peaking and enhancement of high energy emissions at the forward angles, and at backward angles the angular distributions become flat or slightly backward peaked. In Fig. 1 some energy spectra are shown for ^{12}C and ^{19}F reactions, and in Refs. 9 and 11 some results are shown for ^{40}Ar reactions. Comparisons of these spectra show that for a given reaction their shapes are essentially independent of angle (for $\theta_{\text{c.m.}} > 100^\circ$). Also the spectral shapes are almost independent of target projectile combinations for a given excitation energy of the compound nucleus. These features indicate that these H/He emissions are from essentially equilibrated systems. Therefore we assume complete equilibrium and fit the back-angle differential cross sections to an equation from the statistical model.¹⁶

$$W(\theta_{\text{c.m.}}) = W_0 \exp[-(\beta_2/2)\sin^2(\theta_{\text{c.m.}})] \\ \times I_0[(\beta_2/2)\sin^2(\theta_{\text{c.m.}})], \quad (1)$$

where W_0 and β_2 are free parameters and I_0 is the zeroth order modified Bessel function. Only for some of the ^{40}Ar reactions was the anisotropy parameter β_2 determined well enough to warrant any discussion.¹¹ In this work we have sought only the angle and energy integrated evaporative component. For ^{40}Ar induced reactions the large c.m. velocity, along with the detection threshold, cut off

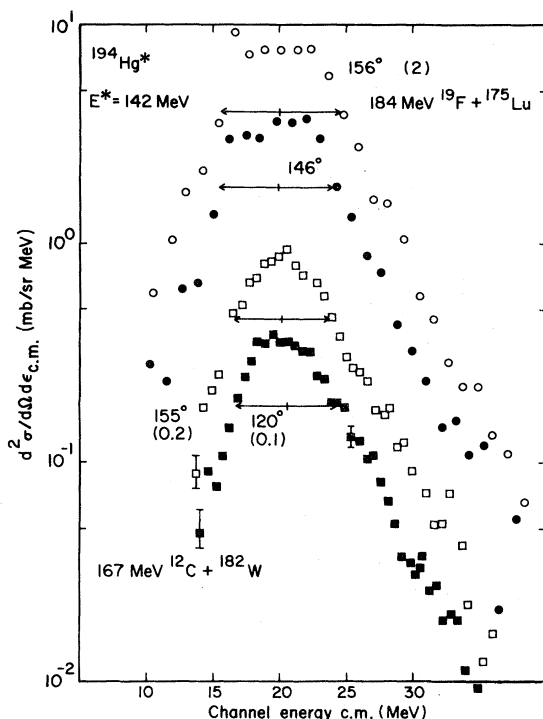


FIG. 1. Energy spectra at back angles for ^4He produced by two different entrance channels (squares, $^{12}\text{C} + ^{182}\text{W}$; circles, $^{19}\text{F} + ^{175}\text{Lu}$). Three of the data sets have been multiplied by the factors shown in parentheses. Arrows denote the FWHM and the cross shows its midpoint for each spectrum.

the low-energy part of the spectra for $\approx 140^\circ - 160^\circ$. We have estimated a correction for this effect from the more completely measured spectra at $\approx 120^\circ$; this correction was never more than 10%. In Table I the H/He cross sections represent the evaporative components only, as obtained by integration of Eq. (1) after fitting to our experimental data. The major source of uncertainty in these evaporative cross sections for ^4He and ^1H is attributable to the assignment and separation of the evaporative component. This uncertainty is largely systematic in its nature and is thus difficult to determine. (See the figures and discussion in Ref. 11 for ^{40}Ar reactions. The data shown in Ref. 10 are typical for the lighter projectiles.) Our best estimates are discussed in the Appendix and are given in Table I.

For reactions induced by ^{12}C , ^{19}F , and ^{20}Ne , the fission component was easily identified on a contour plot (GT) of ΔE vs E . For ^{40}Ar beams these contour plots are known to be complicated by projectilelike fragments and targetlike fragments from deeply inelastic reactions.¹⁷ Nevertheless we have assigned a zone on the ΔE - E maps to fissionlike

fragments, but could include some deeply inelastic reaction products. In Ref. 11 we show angular distributions for these fissionlike events from ^{40}Ar induced reactions. Presumably the inclusion of some deeply inelastic reactions leads to the observed increase of the values of $d\sigma/d\theta$ at small angles. For $\langle\theta_{\text{c.m.}}\rangle \approx 60-90^\circ$ one finds many fewer products similar to the projectile and the singles energy spectra of heavy fragments clearly resolve into two components.¹¹ The low-energy targetlike products are well separated in energy from a broad peak for products of intermediate mass. In this angular region we feel that fission can be more easily identified and we have therefore estimated the fission cross section consistently for all the reactions by interpolating $d\sigma/d\Omega$ to $\langle\theta_{\text{c.m.}}\rangle = 90^\circ$ and multiplying by $2\pi^2$ (i.e., we assume $d\sigma/d\Omega \propto 1/\sin\theta_{\text{c.m.}}$).⁹⁻¹¹

Our raw experimental data for the determination of ER cross sections are much the same as those reported by many other workers who have used gas telescopes. (See Ref. 18 for an extensive set of original citations.) Several angular distributions are shown in Fig. 2 and another is given in Ref. 10. An extrapolation (comprising 20-40% of the cross section) had to be made from 3° or 4° to 0° . This extrapolation and other random experimental errors lead to absolute uncertainties of approximately 25% for the integrated ER cross sections. The relative uncertainties are of course, smaller. For the ^{12}C reactions the recoil energies for the ER products after complete fusion approach the energy threshold for the GT; therefore the residual nuclei after incomplete fusion would be at least partially lost below the threshold.^{8,10} We will discuss this point more fully in the next section. For 196 and 221 MeV ^{40}Ar reactions the ER locus comes very close to that for the slit scattering of low-energy ^{40}Ar . For these cases there is a possibility that some of the ER products were obscured and omitted from the cross sections we report. This is an important experimental point to try to clarify, as will become clear in the next section. At somewhat lower energies Stokstad *et al.*¹⁹ report much larger ER cross sections than we find for $^{40}\text{Ar} + ^{154}\text{Sm}$.

Table I presents a summary of the cross sections for evaporation residues, fission, and evaporative H and He. Some of these results were presented earlier^{10,11} and a few have been modified slightly by averaging with more recent determinations. Fusion cross sections are taken as the sum of those for fusion and evaporation residues. The cumulative decay fraction (CDF) for each product is simply its cross section divided by the fusion cross section

TABLE I. Experimental results for ^{194}Hg compound nuclei. + indicates upper limit.

Beam Target	The reaction systems											
	^{12}C ^{182}W	^{20}Ne ^{174}Yb	^{40}Ar ^{154}Sm	^{12}C ^{182}W	^{19}F ^{175}Lu	^{40}Ar ^{154}Sm	^{12}C ^{182}W	^{19}F ^{175}Lu	^{40}Ar ^{154}Sm	^{20}Ne ^{174}Yb	^{40}Ar ^{154}Sm	^{40}Ar ^{154}Sm
E_{lab} (MeV)	77	104	121	135	98	100	142	142	141	252	194	340
E^* (MeV) ^a	57	82	98	98	80	80	142	142	141	194	194	195
Cross sections ^b (mb), $^4\text{He}/^3\text{H}$ ratio, l_{cr} and l_{ER}												
^1H	204(11)	114(11)	55 +	266(11)	214(11)	73.5 +	544(11)	490(11)	242(11)	1189(11)	703(11)	703(11)
^2H	27(15)	6.0(15)	2.8 +	24(15)	25(15)	6.7(15)	65(15)	87(15)	31.4(15)	189(15)	108(15)	108(15)
^3H	9(20)	2.4(20)	1.09 +	11(20)	10(20)	2.9(20)	32(20)	51(20)	15.6(20)	104(20)	66(20)	66(20)
^4He	31(8)	73(8)	37(8)	176(8)	152(8)	77(8)	387(8)	354(8)	232(8)	984(8)	624(8)	624(8)
ER	545(10)	291(10)	94(10)	458(10)	351(10)	86(10)	539(10)	312(10)	79(10)	225(10)	124(10)	124(10)
Fission	23(8)	663(8)	500 ^c	607(8)	780(8)	754(8)	861(8)	1066(8)	919(8)	985(8)	1439(8)	1439(8)
$^4\text{He}/^3\text{H}$	568(10)	805(7)	594(7)	1065(6)	1131(6)	840(7)	1400(6)	1378(6)	998(7)	1210(7)	1563(8)	1563(8)
l_{cr}	0.61(14)	0.64(14)		0.66(14)	0.71(14)		0.71(14)	0.72(14)	0.96(14)	0.83(14)	0.89(14)	0.89(14)
l_{ER}	36	53	66	45	59	83	65	76	101	85	142	142
	25	29	26	29	32	26	37	36	28	36	39	39
Cumulative decay fractions (CDF) ^d												
^1H	0.25(13)	0.12(13)	0.093(13)	0.25(13)	0.19(13)	0.087	0.34(13)	0.36(13)	0.24(13)	0.98(13)	0.45(14)	0.45(14)
^2H	0.034(17)	0.006(16)	0.005(17)	0.02(16)	0.022(16)	0.008(17)	0.04(16)	0.063(16)	0.03(17)	0.16(17)	0.07(17)	0.07(17)
^3H	0.011(21)	0.003(21)	0.002(21)	0.01(21)	0.009(21)	0.003(21)	0.02(21)	0.037(21)	0.016(21)	0.09(21)	0.04(22)	0.04(22)
^4He	0.055	0.15(11)	0.062(11)	0.17(10)	0.13(10)	0.092(11)	0.24(10)	0.26(10)	0.23(11)	0.81(11)	0.40(11)	0.40(11)
ER	0.96(1)	0.59(5)	0.16(11)	0.43(7)	0.31(9)	0.10(12)	0.39(8)	0.23(10)	0.08(12)	0.186(10)	0.08(12)	0.08(12)
Fission	0.04(12)	0.41(8)	0.84(2)	0.57(6)	0.69(4)	0.90(1)	0.62(5)	0.77(3)	0.92(1)	0.81(2)	0.92(1)	0.92(1)

^a Q values were taken from A. H. Wapstra and K. Bos, *At. Nucl. Data Tables* **19**, 175 (1977); W. D. Myers, *Droplet Model of Atomic Nuclei* (IFI/Plenum, New York, 1977).

^bCross sections for ^1H , ^2H , ^3H , and ^4He emission have been integrated for the evaporative component only, as described in the text. The numbers in parentheses are the estimated uncertainties (in percent) relative to others for the same reaction. The Appendix gives a discussion of these uncertainties (type I in Table III). See text for discussion of possible interferences of (a) slit scattering on ER determinations for 196 and 221 MeV ^{40}Ar and (b) the possibility of some deeply inelastic reactions being included with fission for 340 MeV ^{40}Ar .

^cThis value was not measured; it was interpolated from our data and those in Ref. 19.

^d $\text{CDF}_i = \sigma_i / \sigma_{\text{cr}}$.

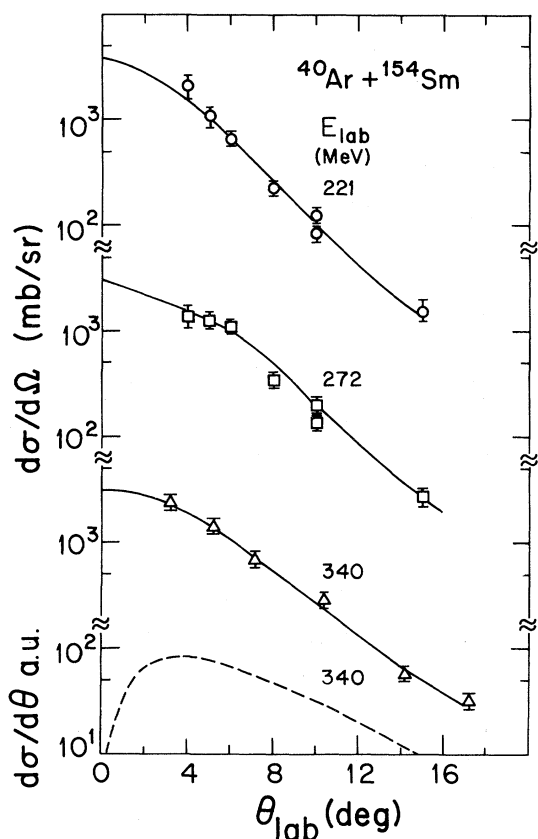


FIG. 2. Angular distributions for evaporation residues from reactions of ^{40}Ar with ^{154}Sm . Statistical uncertainties are shown for each experimental point, smooth curves were drawn for $d\sigma/d\Omega$ and then converted into $d\sigma/d\theta$ as shown for one case.

(σ_{cf}). The values of the critical l for fusion (l_{crit}) and for evaporation residues (l_{ER}) were obtained from the sharp cutoff equations

$$\sigma_{cf} = \pi\lambda^2(l_{crit} + 1)^2 \quad (2)$$

and

$$\sigma_{ER} = \pi\lambda^2(l_{ER} + 1)^2. \quad (3)$$

Energy and spin dependence of these quantities is discussed in the next section. The values of σ_{cf} or σ_{ER} divided by $\pi\lambda^2$ can, of course, be considered dimensionless cross sections with much greater significance than implied by the term "sharp cutoff model." One might say that l_{crit} (or l_{ER}) represents the effective number of partial waves that must be involved in fusion (or ER) reactions, with the understanding that higher partial waves may also be involved but with decreasing probability.

As mentioned in Ref. 10, the coincidence data for ^{12}C and ^{19}F reactions are of limited statistical signi-

ficance. Nevertheless we were able to set an upper limit of $\approx 5\%$ on the fraction of fission in coincidence with H/He for 121 MeV ^{12}C and 135 MeV ^{19}F . This upper limit precludes a significant contribution from H/He evaporation before fission or from the fission fragments for these cases. For the high energies, however, a significant fraction of the H/He evaporation can be accompanied by fission. For example, for 340 MeV $^{40}\text{Ar} + ^{154}\text{Sm}$ about three-fourths of the evaporated ^1H and ^4He were found to be in coincidence with fission.¹¹ It is important to establish whether these emissions occur from the fission fragments or from the reaction complex prior to scission. As discussed in Refs. 9 and 11 there are three pieces of evidence that indicate the heavy predominance of precission H/He evaporation: (1) The energy spectra for ^1H and ^4He in coincidence with a fission product do not exhibit the kinematic shifts expected for evaporation from moving fission fragments (340 MeV $^{40}\text{Ar} + ^{154}\text{Sm}$). Instead they are very similar to the spectra in the singles mode. (See Fig. 6 from Logan *et al.*¹¹) (2) The ratios of ^4He to ^1H are very large (> 0.6) for all the reactions leading to $^{194}\text{Hg}^*$. Such ratios would imply unreasonably large spins if emission were from a fission fragment (see the discussion in Refs. 15 and 16 and that of Fig. 5 later). (3) The shapes of the observed singles spectra, especially for ^4He , are quite different from those calculated from a kinematic simulation of evaporation from fission fragments. Figure 3 shows such a comparison for one case. The smooth curves for the kinematic simulations are invariably broader than the measured spectra and are steeper at high energies. This is a general result of the random vector additions of the velocities of fission fragment and evaporated particle.⁹⁻¹¹ All the measured singles spectra (for $\theta_{c.m.} > 100^\circ$) have shapes typical of evaporation from a compound nucleus as shown in Fig. 1 and Refs. 9 and 11. These shapes *cannot* be reconciled with evaporation from the moving fragments, and they convince us that, in general, He emission from the composite system $^{194}\text{Hg}^*$ predominates over emission from fission fragments. The kinematic comparison does not preclude extensive evaporation of ^1H from the fission fragments, but it seems unlikely that this mechanism dominates for these reactions.

IV. DISCUSSION

A. Some comparisons to other work

In Fig. 4 we show excitation functions for the various observed products for one reaction system,

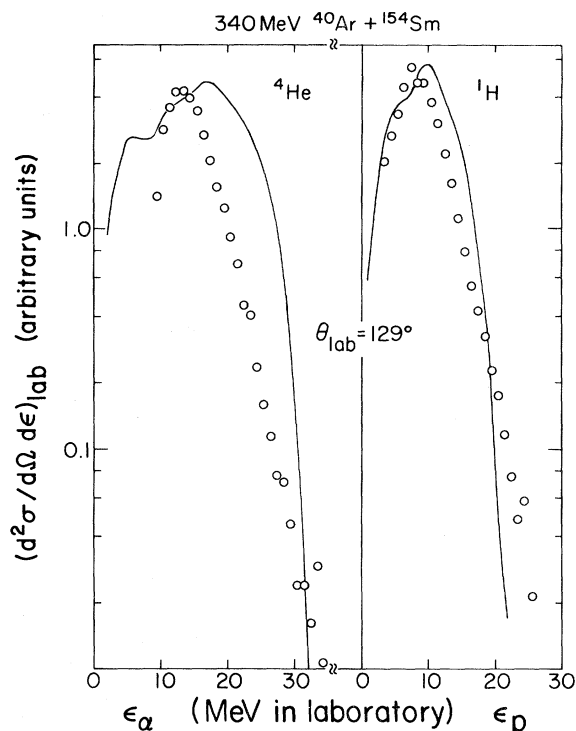


FIG. 3. Typical energy spectra for ${}^1\text{H}$ and ${}^4\text{He}$ from the reaction $340 \text{ MeV } {}^{40}\text{Ar} + {}^{154}\text{Sm}$. Experimental points are compared to smooth curves calculated by a Monte Carlo simulation of evaporation from fission fragments. Gaussian distributions were assumed for the mass and total energy distributions in fission with standard deviations of 24 mass units and 12 MeV, respectively. Angular distributions for each fission product were taken to be $1/\sin\theta_{c.m.}$ and isotropic for H/He. The evaporation spectra were taken as $P(\epsilon) \propto (\epsilon - B) \exp(-\epsilon/T)$ with barrier parameter B from Ref. 18 and T from Ref. 11.

${}^{12}\text{C} + {}^{182}\text{W}$. Our lowest incident energy, 77 MeV, is well above the barrier, so the fusion cross section rises relatively slowly with increasing energy.¹⁸ The balance between fission and ER formation is, however, very strongly energy dependent. Our fission cross sections near 120 MeV are $\approx 20\%$ smaller than the previous measurements of Sikkeland *et al.*²⁰; near 80 MeV we are in reasonable agreement with both Ref. 20 and with recent data from Chalk River.²¹ Excitation functions for fission of ${}^{194}\text{Hg}^*$ and some lighter compound systems have been analyzed previously by use of the equilibrium statistical model.^{22–24} Our addition of data for evaporation residues and light charged particle evaporation brings some interesting new constraints to such an analysis. We will discuss some of these

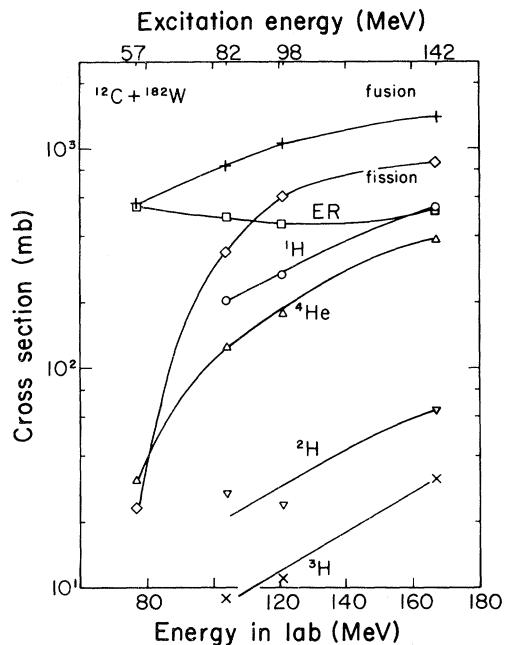


FIG. 4. Excitation functions for fusion, +; fission, \diamond ; ${}^1\text{H}$, \circ , ${}^4\text{He}$, \triangle ; ${}^2\text{H}$, ∇ ; ${}^3\text{H}$, \times ; and evaporation residues ER, \square for the reaction system ${}^{12}\text{C} + {}^{182}\text{W}$. See the Appendix for estimates for the uncertainties.

constraints in a following paper²⁵; here we focus on the phenomenology of fusion and the spin and energy dependence of the ER cross sections.

B. Complete and incomplete fusion and the postulate of a critical distance

In Refs. 8 and 11 we have discussed the conceptual problems that may result from the combined presence of complete and incomplete fusion reactions. For the data given in Table I, the values of σ_{CF} probably include both these processes for ${}^{19}\text{F}$, ${}^{20}\text{Ne}$, and ${}^{40}\text{Ar}$ induced reactions.¹¹ For the reactions induced by 77, 104, and 121 MeV ${}^{12}\text{C}$, the mean recoil energies of the evaporation residues are rather close to the detection threshold for the GT. If a fast forward-peaked proton or α particle is emitted, then the heavy residue might well go undetected. Therefore, it is not really evident what constitutes “complete fusion” from either the theoretical or the experimental viewpoint. Nevertheless in Table II we do make comparisons of our measured fusion cross sections to those calculated by the critical distance postulate.²⁶

The calculated cross sections all employ a critical

TABLE II. Experimental and calculated^a fusion cross sections, σ_{cf} (mb).

E_{lab} (MeV)	$[\sigma_{cf}^{\text{expt}}]^b$ (mb)	Calculated				
		Ngô (Ref. 26)	Ngô (Ref. 27)	Wilczyńska (Ref. 28)	Blocki (Ref. 29)	Vaz (Ref. 18) ^c
$^{12}\text{C} + ^{182}\text{W}$						
77	568	941*		871*	802	983*
104	805	1348	1330	1273	1201	1331
121	1065	1438	1422	1373	1312	1424
167	1400	1590	1578	1543	1499	1580
$^{19}\text{F} + ^{175}\text{Lu}$						
135	1131	1138	1159	1201	1057	1121
184	1378	1406	1421	1452	1347	1393
$^{20}\text{Ne} + ^{174}\text{Yb}$						
125	954	876	944	963	794	856
252	1210	1525	1558	1568	1484	1515
$^{40}\text{Ar} + ^{154}\text{Sm}$						
196	594	548	626	836	545	519
221	840	760	829	1015	757	734
272	998	1072	1128	1279	1069	1051
340	1563	1342	1387	1508	1340	1325

^aCalculations of σ_{cf} as described in Ref. 18 (with the code FRANPIE) with the choice of nuclear potential indicated. The critical distance hypothesis was used with $R_{\text{crit}} = 1.0 (A_{\text{tgt}}^{1/3} + A_{\text{proj}}^{1/3})$ fm for energies above the transition energy for each potential [$\sigma_{cf} = \pi R_{\text{crit}}^2 (1 - V(R_{\text{crit}})/E_{\text{c.m.}})$]. For the cases denoted by an asterisk the incident energy is less than the transition energy and the partial wave summation [$\sigma_{cf} = \pi \lambda^2 \sum (2l+1) T_l$] was made as described in Ref. 18. The transition energy is defined by the condition $E_{\text{c.m.}} = V_{\text{NCl}}(R_{\text{crit},l}) = V_{\text{NCl}}(R_{\text{max},l})$, where V_{NCl} is the Coulomb plus nuclear plus centrifugal potential and R_{max} is the radial distance of the barrier maximum.

^bAbsolute uncertainties in σ_{cf} are $\approx 25\%$ as discussed in the Appendix.

^cTabulated proximity potential empirically adjusted to match fusion barriers by using Eq. (11) of Ref. 18.

radius of $1.00 (A_t^{1/3} + A_p^{1/3})$ fm and a point charge Coulomb potential, but they employ a variety of nuclear potentials.^{18,26-29} At the high energies used in this work there is rather little dependence of the calculated values on the choice of nuclear potential used or (for the proximity potential) on its empirical adjustments (see footnote to Table II). The measurements for ^{19}F , ^{20}Ne , and ^{40}Ar projectiles are all rather close to the calculated values. However, for ^{12}C the measured cross sections, especially at the lower energies, are much smaller than those calculated. The recoil energies for the heavy residuals are lowest for the ^{12}C induced reactions, and thus they would be most easily eliminated by the detection threshold. Any forward-peaked light particle accompanying a partial fusion reaction could easily take away enough momentum to exclude the heavy recoil from detection. The heavier projectiles (^{19}F , ^{20}Ne , and ^{40}Ar) have considerably greater momenta and such momentum loss from light particle emission has much less chance of eliminating the associated incomplete fusion residues from detection.^{8,10}

Our inference from these considerations is that, for ^{19}F , ^{20}Ne , and ^{40}Ar induced reactions, we detect complete plus incomplete fusion and that for ^{12}C we omit the latter. Correspondingly the empirical r_{crit} value of 1.0 fm has been established by data that probably include both complete and incomplete fusion.²⁶ Therefore this postulate predicts our results rather well for all but ^{12}C reactions, for which the measurements may well eliminate the incomplete fusion. This is a point of some significance for the use of the critical distance idea to estimate apparent critical angular momentum (l_{crit}) or the corresponding cross sections for fusion.

The problems posed by significant occurrence of both complete and incomplete fusion can only be answered by extensive observations of the direct particle emission. As discussed more completely in Ref. 8, the measured cross sections for ER and fission are not sufficient to give the exact cross sections, l_{ER} and l_{crit} values for formation of compound nuclei at full excitation energy. Nevertheless the best approximation at present seems to be the

standard procedure [embodied in Eqs. (2) and (3)]. We will use these equations to give guidelines for the spin distributions in the reactions of interest here.

C. The ratio of evaporative ${}^4\text{He}$ to ${}^1\text{H}$

In Fig. 5 we show the observed ratios of evaporative ${}^4\text{He}$ to ${}^1\text{H}$ as a function of l_{crit} for ${}^{194}\text{Hg}^*$ as compared to data for other reaction systems. The results for ${}^{194}\text{Hg}^*$ and the other rather heavy composite systems (${}^{204}\text{Po}^*$ and ${}^{237}\text{Bk}^*$) (Ref. 11) are quite different from those for the lighter systems ${}^{75}\text{Br}^*$ and ${}^{117}\text{Te}^*$.^{12,15,16} The heavy systems have ${}^4\text{He}/{}^1\text{H}$ ratios that are large (>0.5) and only slowly varying with E^* or l_{crit} . The lighter ones have ${}^4\text{He}/{}^1\text{H}$ ratios that change by twofold as l_{crit} is increased by $\approx 30\hbar$ and no clear dependence on E^* . The system ${}^{156}\text{Er}^*$ is of intermediate character.¹¹ We have used these differences as the basis for an argument against H/He evaporation from fission fragments^{9,11} which we expect to be similar to ${}^{75}\text{Br}^*$ and ${}^{117}\text{Te}^*$. This argument assumes that these ratios do not change drastically from the neutron deficient Br and Te systems studied previously to the more neutron rich fission products studied here.^{2,9,30} Similarity in the mass dependence for ${}^1\text{H}$ and ${}^4\text{He}$ separation energies provides the basis for this assumption.⁹ It should, of course, be tested by experimental measurements.

D. Energy and spin dependence of l_{ER}

Figure 6 shows our data for σ_{ER} compared to similar data from other studies.^{17,31-33} Before ad-

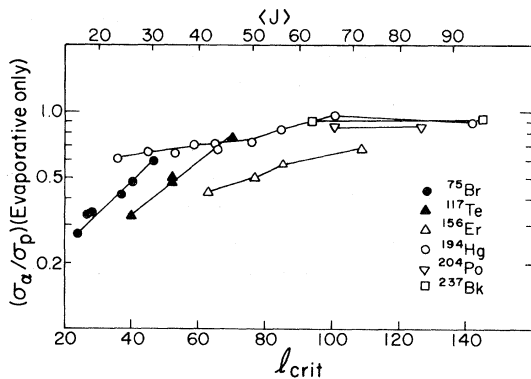


FIG. 5. Ratio of evaporative ${}^4\text{He}$ to ${}^1\text{H}$ from direct observation as given in Table I. (Data from this work and Refs. 11, 12, and 15.) The uncertainties are about $\pm 14\%$ for each point.

ressing this figure directly let us review the simplified qualitative statistical model used by many for a first orientation to such data.³⁴ One writes a Boltzmann expression for the width (or decay probability) ratio

$$\Gamma_f/\Gamma_n \approx \exp - \{ [B_f(J) - B_n] / T \},$$

where B_f is the fission barrier and B_n the neutron binding energy and $\Gamma_n \gg \Gamma_p$ or Γ_α . Thus one expects a sharp change in Γ_n/Γ_f at the spin J where $B_f(J) \approx B_n$. Increasing excitation energy E^* raises T (as $E^* \approx aT^2$) and broadens the transition region of spins where fission and evaporation have comparable widths. The rotating liquid drop model (RLDM) (Ref. 24) can be used to estimate $B_f(J)$ [for ${}^{194}\text{Hg}^*$ RLDM gives $B_f(J=0) \approx 15$ MeV and $J \approx 40$ for $B_f(J) = B_n$]. Thus one expects fission to remove the high-spin compound nuclei before any

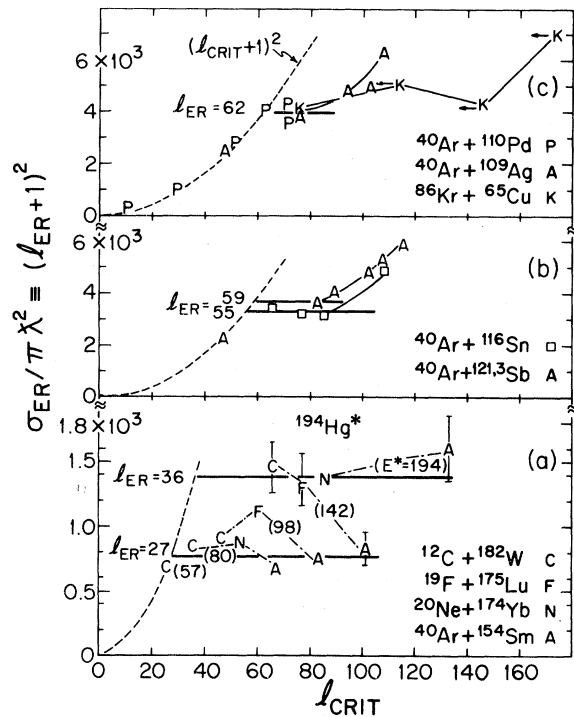


FIG. 6. The dimensionless evaporation residue cross section $\sigma_{\text{ER}}/\pi\lambda^2$ vs l_{crit} for several reactions as indicated. The dotted lines show $(l_{\text{crit}} + 1)^2$, which must represent the data when fission is negligible. Solid lines are drawn for the l_{ER} values indicated. (a) Data from this work. The uncertainties are $\pm 15\%$ as discussed in the Appendix. Excitations energies are noted for reactions leading to ${}^{194}\text{Hg}^*$. (b) Data from Refs. 11, 32, and 33. (c) Data from Refs. 17 and 31. For the Kr reactions the l_{crit} values are upper limits but the σ_{ER} values are unambiguous.

particle evaporation. For the survivors of lower spin the RLDM predicts that B_f decreases as Z^2/A increases, and therefore along a neutron-evaporation cascade the fission barrier will be slightly decreased after each step and fission will slightly deplete the surviving population of evaporation residues.

References 23 and 34 have used this simple, qualitative picture to discuss data on fission and evaporation residues for compound nuclei of $A \approx 150$. The qualitative pattern of the data for their cases and for this $^{194}\text{Hg}^*$ study is quite similar. At first glance the values of l_{ER} (see Table I) seem to vary only slowly with excitation energy or l_{crit} (for entrance channels with $l_{\text{crit}} > l_{\text{ER}}$). The hypothesis of Britt *et al.*³⁴ was that there must be a very abrupt increase in fission probability for the spin where $B_f(J) = B_n$. Even for the first step of fission-evaporation competition many of the high spin compound nuclei are expected to be removed by fission. Successive steps in the competitive decay also lead to losses to fission of remaining nuclei that are characterized by the highest spins. The low-spin fraction of evaporating nuclei is not expected to be reduced appreciably by the successive fission-evaporation competition, and thus $\sigma_{\text{ER}}/\pi\lambda^2$ or l_{ER} should be almost energy independent. This is a very different situation from that for actinide fission where $B_f(J=0) \lesssim B_n$, and the residual-nucleus population for the whole range of spins is heavily reduced by fission competition at each step.³⁵ Such a reduction in the fission survival population would lead to a steady decrease of σ_{ER} (and the inferred values of l_{ER}) with increasing E^* .

The observed values of σ_{ER} for $^{194}\text{Hg}^*$ present a much more complicated picture from that described above, as we can see from the plots in Fig. 6(a). The lower envelope of the data points for σ_{ER} for $^{194}\text{Hg}^*$ in Fig. 6(a) is consistent with an energy independent value of l_{ER} for the initial spin for $^{194}\text{Hg}^*$ ($l_{\text{ER}} = 27$). By the above argument fission dominates the decay for initial spins > 27 . However, there are four data points for which the observed ER cross sections are too large to be reconciled with this idea and an l_{ER} value of 27. The values of $\sigma_{\text{ER}}/\pi\lambda^2$ for $E^* = 142$ MeV indicate an interesting dependence on the entrance channel; the 272 MeV ^{40}Ar induced reaction ($l_{\text{ER}} = 28$) is consistent with the bulk of the data that have $l_{\text{ER}} \approx 27$, but σ_{ER} or l_{ER} values for 167 MeV ^{12}C and 184 MeV ^{19}F are much larger ($l_{\text{ER}} = 37$ and 36). The results for $E^* = 194$ MeV indicate an interesting dependence on incident energy; both the ^{20}Ne and the ^{40}Ar reactions give values of σ_{ER} or l_{ER} that are decidedly

large ($l_{\text{ER}} = 36$ and 39) compared to the trend from lower energies (i.e., $l_{\text{ER}} = 27$).

It is important to recognize that the variation in these values of l_{ER} or $\sigma_{\text{ER}}/\pi\lambda^2$ (for fixed E^*) cannot be ascribed to a simple failure of the sharp cutoff approximation. Even if the fission survival probability $W_{\text{ER}}(J, E^*)$ is a slowly varying function of spin, we expect $\sigma_{\text{ER}}/\pi\lambda^2$ to be essentially independent of entrance channel. This expectation follows from the Bohr independence hypothesis^{12,25} that $W_{\text{ER}}(J, E^*)$ is a property of the equilibrated compound nucleus [with values expected to be close to unity at low spin (say < 27) and with lower values at high spin]. The fact that $\sigma_{\text{ER}}/\pi\lambda^2$ (for $E^* = 142$ MeV) is not constant demands that $W_{\text{ER}}(J, E^*)$ differ for each entrance channel and that therefore the intermediate transition complex be not fully equilibrated. Two obvious nonequilibrium mechanisms that could contribute to these observations are as follows: (a) Incomplete fusion reactions may contribute more to ER for ^{12}C and ^{19}F than for ^{40}Ar .⁸ (b) Deeply inelastic reactions may occur for entrance channel $l \approx 30$ more frequently for ^{40}Ar than for ^{19}F or ^{12}C . Agarwal *et al.* have studied this kind of nonequilibrium but fissionlike reaction.³⁶ We cannot distinguish these possibilities, but in any case our results require some mechanism not involving complete equilibrium between excitation modes that lead to fissionlike decay and those leading to ER production (presumably particle emission). The surprising point here is that these effects are apparent in the ER production thought to concern spins of ≈ 30 . Both incomplete fusion and nonequilibrium fission are usually thought to be associated with much larger spins. Another possible explanation for these observations involves the evaporative H/He; it will be discussed in another paper.²⁵

Our data for $^{194}\text{Hg}^*$ [Fig. 6(a)] indicate that a large increase in $\sigma_{\text{ER}}/\pi\lambda^2$ occurs for ^{40}Ar at $l_{\text{crit}} \approx 110$; for $^{19}\text{F}/^{20}\text{Ne}$ at $l_{\text{crit}} \approx 50$; for ^{12}C at $l_{\text{crit}} \approx 40$. For comparison we have plotted data for several other reactions in the same way [see Figs. 6(b) and (c)]. For $^{40}\text{Ar} + ^{110}\text{Pd}/^{109}\text{Ag}$ there appears to be a narrow plateau for $\sigma_{\text{ER}}/\pi\lambda^2 \approx 4000$ for $60 \leq l_{\text{crit}} \leq 90$; then a decided increase. A very similar composite system is formed by $^{86}\text{Kr} + ^{65}\text{Cu}$; the abrupt increase here occurs for $l_{\text{crit}} \leq 150$. Each of the other ^{40}Ar reactions seems to show a break for $l_{\text{crit}} \approx 80$. In sum, all the results point to a distinct rise in $\sigma_{\text{ER}}/\pi\lambda^2$ for large values of l_{crit} (and/or E^*). The value of l_{crit} for this breakaway changes with the target-projectile combination from ≈ 40 for ^{12}C

to $\approx 80-110$ for ^{40}Ar to ≈ 150 for $^{86}\text{Kr} + ^{65}\text{Cu}$.

This increase with excitation energy or l_{crit} for $\sigma_{\text{ER}}/\pi\lambda^2$ (or l_{ER}) is equivalent to an increase in the average number of partial waves that finally survive fission and lead to ER's. In other words the fission competition for high J (J greater than the l_{ER} at the plateau) has become less effective with increasing excitation energy. A natural inference is that this effect may well be related to the increase in light charged particle production as mentioned by Britt *et al.*³⁴ (either evaporated or direct or both). The emission of H/He in massive transfer (or incomplete fusion) is generally thought to arise from entrance channel l values near to l_{crit} . As $l_{\text{crit}} \gg l_{\text{ER}}$ one would expect that the high spin residual nucleus would usually undergo fission. For example, consider $340 \text{ MeV } ^{40}\text{Ar} + ^{154}\text{Sm} \rightarrow ^{194}\text{Hg}$ ($E^* = 195 \text{ MeV}$). The value of l_{crit} is 142 and that for l_{ER} is 39. It seems unlikely that H or He emission from massive transfer for $l \approx 142$ could reduce the excitation energy or spin enough to leave the residual nucleus immune to fission competition. Another possibility is that the apparently evaporative H/He emission may reduce the fissility of those Hg composite nuclei with l near to l_{ER} . We will discuss this further in a subsequent paper.²⁵

V. SUMMARY

Twelve reaction systems have been studied that give the composite/compound nucleus $^{194}\text{Hg}^*$. Cross sections are presented for the production of evaporative H/He, fission, and evaporation residues. The energy spectra and angular distributions of H/He at backward angles have been used to identify H/He emission after thermal equilibration. Several arguments based on our data rule our evaporation from the fission fragments as an important deexcitation mechanism. Systematic behavior of the ER cross sections reveals two interesting features:

(1) Nonequilibrium mechanisms affect the ER production: Either incomplete fusion directly feeds the ER's or nonequilibrium fission competes with ER formation. Our expectation was that such fast nonequilibrium reactions would be localized on partial waves near l_{crit} (or ≥ 59) and would not affect ER production from much smaller l waves.

(2) Fission in competition with evaporation residue production becomes weaker for excitation energies $> 100 \text{ MeV}$. This fact, revealed by increasing values of $\sigma_{\text{ER}}/\pi\lambda^2$, is accompanied by increasing

H/He production and may be caused by their removal of charge, energy, and angular momentum from the composite nuclei.

ACKNOWLEDGMENTS

This project was supported in part by the Division of Nuclear Physics of the U. S. Department of Energy and by CRNS of France. The staffs of the SuperHILAC and 88 inch cyclotron at the Lawrence Berkeley Laboratory have been very helpful. We are grateful to D. Guerreau, E. Duek, L. Kowalski, Y. LeBeyec, and A. Fleury for helpful discussions and assistance in many ways.

APPENDIX: PROCEDURES FOR DATA COLLECTION AND ANALYSIS AND ESTIMATES OF THE RELEVANT UNCERTAINTIES

This work reports on a long series of experiments carried out between 1976 and 1979; experimental arrangements and methods have been described in Refs. 8–11 and in Sec. II. The earlier experiments, reported in Ref. 10 (^{12}C of 121 and 167 MeV and ^{19}F of 135 and 184 MeV), had somewhat lower standards for verification by redundancy as compared to the latter ones reported here and in Ref. 11. In this Appendix we try to estimate the various uncertainties applicable for the latter experiments. It is possible that some additional systematic uncertainties may obtain for the earlier experiments.

In Table III we give a list of estimated uncertainties from various sources for each of the products that we study. A blank entry means that we consider a particular source of uncertainty to be negligible for that product. For the ER cross sections we normally used the ratio of ER to elastic scattering as measured simultaneously in the same telescope. This procedure cancels many of the possible sources of error. We then drew a smooth curve by eye for $d\sigma/d\Omega_{\text{ER}}$ and extrapolated it to zero degrees as shown in Fig. 2. The shapes of these curves result from a combination of the reaction kinematics and the small angle scattering in the target; we expect them to have very similar shapes but to become progressively more narrow with increasing recoil energy of the ER. As we use the same procedure for extrapolation to zero degrees for each measurement, we expect the relative errors to be significantly less than the absolute errors. There are some special systematic errors that could obtain for ^{12}C and

TABLE III. Estimates of uncertainties for each product from various sources.

Type of uncertainty	ER	Fission	^4He	^1H	^2H	^3H
(A) Identification of desired product	$^{12}\text{C}^{\text{a}}$, 196, 221 MeV $^{40}\text{Ar}^{\text{b}}$	$^{40}\text{Ar}^{\text{c}}$			15%	15%
(B) Threshold consistency for energy integration				5%	5%	5%
(C) Blank subtraction				5%	10%	10%
(D) Dead time correction		3%	3%	3%	3%	3%
(E) Beam monitor (Faraday cup or elastic)		7%	7%	7%	7%	7%
(F) Target thickness and detector apertures		10%	10%	10%	10%	10%
(G) Statistics (per datum) ^d	~10%	<3%	<3%	<3%	<6%	<10%
(H) Transformation to c.m.		<5% ^e	<2%	<2%	<2%	<2%
(H) Form of fitting function	See Fig. 2 ^f	$1/\sin\theta$	Eq. (1)	Eq. (1)	Eq. (1)	Eq. (1)
(J) Precision of fit (region of measurement)	<10%	<5%	<5%	<5%	<15%	<20%
Overall estimated uncertainties						
(1) Relative to others for the same reaction ^g	10%	8%	8%	11%	15%	20%
(2) Relative to others for all reactions ^h	15%	13%	13%	15%	18%	22%
(3) Absolute ⁱ	25%	15%	15%	20%	25%	30%

^aThe recoil energies were very low and some incomplete fusion events could well have been lost (see Table II).

^bInterference from slit scattering as described in text.

^cPossible interference by deeply inelastic scattering.

^dTypically 5–15 separate data points were used to fit the desired angular distribution.

^eMeasured in singles and transformed to c.m. by using the mean fission fragment velocity from systematics.

^fExtrapolation of $d\sigma/d\Omega$ to 0° by eye as shown in Fig. 2.

^gIncluding B, D, E.

^hIncluding B, C, D, E.

ⁱIncluding our guess for the integration of the fitting function, but not including interferences on line A.

196/221 MeV ^{40}Ar , as discussed in the text.

For the fission measurements from beams of ^{12}C , ^{19}F , and ^{20}Ne , there is essentially no interference from either the targetlike or the projectilelike fragments. For the ^{40}Ar reactions there may be a mixture of fission and deeply inelastic reactions as discussed in the text. Other workers have discussed the errors of angular integrations for fission products based on the assumption of an angular distribution proportional to $1/\sin\theta$; they are small.^{20,32}

The values of CDF_{ER} in Table I are determined from the following equation:

$$\text{CDF}_{\text{ER}} = \frac{1}{1 + \sigma_{\text{fis}}/\sigma_{\text{ER}}} \quad (4)$$

The relative uncertainties (type 1 below) for σ_{fis} and

σ_{ER} have been used for the error estimate for CDF_{ER} (and similarly for CDF_{fis}).

For the light charged particles, H and He, we have estimated typical uncertainties from various sources. The ^4He determinations are the cleanest as they are most easily identified and least effected by contamination from the target frame. The protons are easily identified and abundant, but they suffer two problems as compared to ^4He . For cyclotron experiments, we do not collimate the beam, and there is often a small beam halo that causes contamination from reactions with the target frame. To correct for this we have made subtractions as determined from blank runs. Even after these subtractions (less than 20% for cyclotron experiments and <10% for the SuperHILAC), the proton spec-

tra do not decrease as rapidly at low energy as do those for ^4He (see Ref. 11). This means that the choice of the low-energy integration limit poses a small problem. We try to select this limit in a consistent way for all the experiments. Compared to ^1H , the ^2H and ^3H suffer by lower abundance; hence they are more subject to contamination by misidentified protons and, of course, have greater statistical uncertainties. Our estimates for other sources of uncertainty are also given in the upper part of Table III.

In the lower part of Table III we estimate the overall uncertainties for the integrated cross sections in three separate ways: (1) relative to others for the same reaction; (2) relative to others for all reactions; (3) absolute. For the quantities in Table I

we are interested in the ratio $^4\text{He}/^1\text{H}$ and the values of CDF; each of these involves cross sections for one reaction, and thus the relevant overall uncertainties are of type 1. In Table II we compare measured cross sections for complete fusion to model calculations; here the absolute uncertainties (type 3) are relevant. In Table I of Ref. 25 we obtain the decay fractions for high spin zones by taking differences between different reactions, and here the relevant uncertainties are of type 2. For Fig. 6 we compare values of $\sigma_{\text{ER}}/\pi\lambda^2$ for different reactions, and here also the type 2 uncertainty is relevant. With these choices of the relevant uncertainties and their estimates from Table III, we have assigned overall errors in the tables and figures.

*Permanent address: Centre d'Etudes Nucléaires de Bordeaux-Gradignan, Laboratoire de Chimie Nucléaire ER4 No. 144, Le Haut Vigneau, 33170 Gradignan, France.

†Permanent address: Laboratoire de Chimie Nucléaire, Institut de Physique Nucléaire, B. P. No. 1, 91406 Orsay, France.

¹D. Bodansky, *Annu. Rev. Nucl. Sci.* **12**, 107 (1962).

²T. D. Thomas, *Annu. Rev. Nucl. Sci.* **18**, 343 (1968).

³A. Fleury and J. M. Alexander, *Annu. Rev. Nucl. Sci.* **24**, 279 (1974).

⁴U. Schröder and J. R. Huizenga, *Annu. Rev. Nucl. Sci.* **27**, 465 (1977); J. Galin, D. Guerreau, and R. Babinet, *J. Phys. Soc. Jpn.* **44**, 683 (1978); V. V. Volkov, *Phys. Rep.* **C44**, 93 (1978).

⁵T. Ericson, *Adv. Phys.* **9**, 423 (1960).

⁶J. M. Miller, G. L. Catchen, D. Logan, M. Rajagopalan, J. M. Alexander, M. Kaplan, and M. S. Zisman, *Phys. Rev. Lett.* **40**, 100 (1978).

⁷M. Rajagopalan, L. Kowalski, D. Logan, M. Kaplan, J. M. Alexander, M. S. Zisman, and J. M. Miller, *Phys. Rev. C* **19**, 54 (1979).

⁸H. Delagrangé, D. Logan, M. F. Rivet, M. Rajagopalan, J. M. Alexander, M. S. Zisman, M. Kaplan, and J. W. Ball, *Phys. Rev. Lett.* **43**, 1490 (1979).

⁹D. Logan, M. Rajagopalan, M. S. Zisman, J. M. Alexander, M. Kaplan, and L. Kowalski, *Phys. Rev. C* **22**, 104 (1980).

¹⁰J. M. Miller, D. Logan, G. L. Catchen, M. Rajagopalan, J. M. Alexander, M. Kaplan, J. W. Ball, M. S. Zisman, and L. Kowalski, *Phys. Rev. Lett.* **40**, 1074 (1978).

¹¹D. Logan, H. Delagrangé, M. F. Rivet, M. Rajagopalan, J. M. Alexander, M. Kaplan, M. S. Zisman, and E. Duek, *Phys. Rev. C* **22**, 1080 (1980); and additional measurements of out-of-plane correlations by M. F. Rivet, D. Logan, J. M. Alexander, D. Guerrau, E.

Duek, M. S. Zisman, and M. Kaplan *Phys. Rev. C* **25**, 2430 (1982), the following paper.

¹²See for example, R. C. Reedy, M. J. Fluss, G. F. Herzog, L. Kowalski, and J. M. Miller, *Phys. Rev.* **188**, 1771 (1969); A. M. Zebelman, L. Kowalski, J. M. Miller, K. Beg, Y. Eyal, G. Yaffe, A. Kandil, and D. Logan, *Phys. Rev. C* **10**, 200 (1974).

¹³M. M. Fowler and R. C. Jared, *Nucl. Instrum. Methods* **124**, 341 (1975).

¹⁴See particularly H. C. Britt and A. R. Quinton, *Phys. Rev.* **124**, 877 (1961).

¹⁵J. Galin, B. Gatty, D. Guerreau, C. Rousset, U. C. Schlotthauer-Voos, and X. Tarrago, *Phys. Rev. C* **9**, 1113 (1974); **9**, 1126 (1974); **10**, 638 (1974); R. Babinet, B. Cauvin, J. Girard, J. M. Alexander, T. H. Chiang, J. Galin, B. Gatty, D. Guerreau, and X. Tarrago, *Z. Phys. A* **295**, 153 (1980); D. Guerreau and R. Babinet *J. Phys. C* **10**, 217 (1980).

¹⁶T. Døssing, private communication; G. L. Catchen, M. Kaplan, J. M. Alexander, and M. F. Rivet, *Phys. Rev. C* **21**, 940 (1980).

¹⁷See, for example, H. C. Britt, B. H. Erkkilä, R. H. Stokes, H. H. Gutbrod, F. Plasil, R. L. Ferguson, and M. Blann, *Phys. Rev. C* **13**, 1483 (1976); F. Plasil, R. L. Ferguson, H. C. Britt, B. H. Erkkilä, P. D. Goldstone, R. H. Stokes and H. H. Gutbrod, *ibid.* **18**, 2603 (1978).

¹⁸L. C. Vaz and J. M. Alexander, *Phys. Rev. C* **18**, 2152 (1978); L. C. Vaz, J. M. Alexander, and G. R. Satchler, *Phys. Rep.* **69**, 373 (1981).

¹⁹R. G. Stokstad, W. Reisdorf, K. D. Hildenbrand, J. V. Kratz, G. Wirth, R. Lucas, and J. Poitou, *Z. Phys. A* **295**, 269 (1980).

²⁰T. Sikkeland, J. E. Clarkson, N. H. Steiger-Shafir, and V. E. Viola, *Phys. Rev. C* **3**, 329 (1971); T. Sikkeland, *Phys. Rev.* **135**, B669 (1964).

²¹J. U. Anderson, A. S. Jensen, K. Jorgensen, E. Laegs-

- gaard, K. O. Nielsen, J. S. Forster, I. V. Mitchell, D. Ward, W. M. Gibson, and J. J. Cuomo, K. Dan. Vidensk. Mat. Fys. Medd. **40**, No. 7 (1980); IAEA Report IAEA-SM/241-C7, 1979.
- ²²H. Delgrange, A. Fleury, and J. M. Alexander, Phys. Rev. C **16**, 706 (1977).
- ²³M. Beckerman and M. Blann, Phys. Rev. Lett. **38**, 272 (1977); Phys. Lett. **68B**, 31 (1977); Phys. Rev. C **17**, 1615 (1978).
- ²⁴S. Cohen, F. Plasil, and W. J. Swiatecki, Ann. Phys. (N.Y.) **82**, 557 (1974).
- ²⁵J. M. Alexander, H. Delgrange, M. Rajagopalan, M. F. Rivet, and L. C. Vaz (unpublished).
- ²⁶J. Galin, D. Guerreau, M. Lefort, and X. Tarrago, Phys. Rev. C **9**, 1018 (1974); D. Glass and U. Mosel, Nucl. Phys. **A237**, 429 (1975); C. Ngô, G. Tamain, M. Beiner, R. J. Lombard, D. Mas and H. H. Deubler, *ibid.* **A252**, 237 (1975); K. A. Bruekner, J. R. Buchler and M. Kelly, Phys. Rev. **173**, 944 (1968).
- ²⁷H. Ngô and C. Ngô, Orsay Report I.P.N.P/TH 80-20, 1980.
- ²⁸K. Siwek-Wilczyńska and J. Wilczyński, Phys. Lett. **74B**, 313 (1978).
- ²⁹J. Blocki, J. Randrup, W. J. Swiatecki, and C. F. Tsang, Ann. Phys. (N.Y.) **105**, 427 (1977).
- ³⁰J. Gilat and J. R. Grover, Phys. Rev. C **3**, 734 (1971).
- ³¹S. Della Negra, H. Gauvin, H. Jungclas, Y. LeBeyec, and M. Lefort, Z. Phys. A **282**, 65 (1977); C. Cabot, H. Gauvin, Y. LeBeyec, H. Delgrange, J. P. Dufour, A. Fluery, Y. Llabador, and J. M. Alexander, J. Phys. C **10**, 234 (1980).
- ³²B. Tamain, C. Ngô, J. Peter, and F. Hanappe, Nucl. Phys. **252**, 187 (1975).
- ³³H. Gauvin, D. Guerreau, Y. LeBeyec, M. Lefort, F. Plasil, and X. Tarrago, Phys. Lett. **58B**, 163 (1975).
- ³⁴The sharp cutoff approximation is often used as a guide. See, for example, Ref. 17 and H. C. Britt, B. H. Erkkila, P. D. Goldstone, R. H. Stokes, B. B. Back, F. Folkmann, O. Christensen, B. Fernandez, J. D. Garrett, G. B. Hagemann, B. Herskind, D. L. Hillis, F. Plasil, R. L. Ferguson, M. Blann, and H. H. Gutbrod, Phys. Rev. Lett. **39**, 1458 (1977); more detailed calculations are discussed similarly by A. Gavron, Phys. Rev. C **21**, 230 (1980).
- ³⁵E. K. Hyde, *The Nuclear Properties of the Heavy Elements III, Fission Phenomena* (Prentice-Hall, Englewood Cliffs, New Jersey, 1964).
- ³⁶S. Agarwal, J. Galin, B. Gatty, D. Guerreau, M. Lefort, X. Tarrago, R. Babinet, and J. Girard, Z. Phys. A **296**, 287 (1980).